GiG Research Institute

JOURNAL OF SUSTAINABLE MINING

Volume 20 | Issue 4 Article 4

2021

Modelling the throttle effect in a mine drift

Modelling the throttle effect in a mine drift

Rickard Hansen

The University of Queensland, Sustainable Minerals Institute, Australia

Abstract

The throttle effect is a phenomenon, which may occur during a fire underground, causing unforeseen smoke spread. This paper focuses on the modelling of the throttle effect in a mine drift, using a CFD software. The aim of the paper is to investigate whether the CFD tool is able to predict and reproduce the throttle effect for fire scenarios underground. Experimental data from fire experiments in a model-scale mine drift and modelling results from a CFD model were used during the analysis. It was found that the CFD model was not able to fully reproduce the throttle effect for fire scenarios in a mine drift. The inability was due to the under prediction of the fire gas temperature at the ceiling level and the over prediction of the temperatures at the lower levels. The difficulties occurred foremost during transient periods with high fire growth rates. Given the difficulties in modelling the thermal stratification and the throttle effect, the use of CFD models should be mainly for qualitative analysis. Quantitative analysis could possibly be performed for non-transient and low intensity fires.

Keywords: throttle effect, fire, mine drift, mass flow, CFD, longitudinal ventilation

1. Introduction

One of the key risks during a fire in an underground mine is the smoke spread, where an unforeseen smoke spread will increase the risks to the mining personnel even further. One of the phenomena which may cause unforeseen smoke spread – initiating disturbances and air flow changes underground – is the throttle effect. The throttle effect will result in a reduction in the mass flow rate, which in turn may cause changes in ventilation flow directions and difficulties during the smoke extraction as well as the evacuation phase.

When designing the fire safety of an underground mine, data from full-scale fire tests performed in similar surroundings and with similar fuel items would be key information. Obviously, performing full-scale fire experiments in an underground mine will be very costly, time consuming, etc. A tool, which could complement – but never fully replace – the full-scale experiments, is a CFD (Computational Fluid Dynamics) tool for modelling a fire underground.

This paper focuses on the modelling of the throttle effect in a mine drift (with a hard rock surface where negligible gas permeability is assumed), using a CFD software tool to reproduce the flow behaviour of earlier conducted fire experiments. Is the CFD tool able to predict and reproduce the throttle effect for fire scenarios underground? Being able to model the throttle effect – using a CFD model – would provide a powerful tool with respect to the fire safety underground. To validate the capability of the CFD tool, experimental data from fire experiments in a model-scale mine drift were applied as these covered essential data for an analysis [1]. The purpose of this paper is to validate the CFD model for fire scenarios with varying conditions, where the CFD model could potentially be a tool in future studies on the fire behaviour underground. During the work, mainly the flow velocity and the temperature distribution were analysed, as these parameters will largely influence the mass flow situation in the mine drift.

A very limited number of earlier studies have been conducted on the throttle effect in underground mines or the use of CFD modelling in mines. No earlier study has been conducted on CFD modelling of the throttle effect in underground mines.

Hwang and Chaiken [2] and Lee et al. [3] studied the interaction between a fire and the airflow in

Received 11 April 2021; revised 15 September 2021; accepted 26 September 2021.
Available online 30 December 2021
E-mail address: rickard.hansen@uq.edu.au.

https://doi.org/10.46873/2300-3960.1329

a duct, analysing the change in the air velocity prior to the fire compared to during the fire. Litton et al. [4] conducted fire experiments to quantify the throttle effect on the ventilation flow and found the overall effects to be substantial. Hansen [5] conducted fire experiments in a model-scale mine drift, investigating the nature of the throttle effect. Vaitkevicius et al. [6] presented a modelling study – using the CFD software FDS (Fire Dynamics Simulator) – to demonstrate the impact of the throttle effect on tunnel fires. The study was entirely based on CFD modelling and no experimental data was applied in the modelling.

Regarding CFD studies in underground mines, Edwards and Hwang [7,8] presented studies on the smoke spread prediction in a mine entry and the fire spread along combustibles in a ventilated mine entry, using a CFD-model. Edwards et al. [9,10] and Friel et al. [11] performed CFD-studies on the critical air velocity and backlayering in a mine entry, a mine section and a crosscut. Trevits et al. [12] conducted a CFD-study on the characteristics of mine fire combustion and flame spread for deep-seated fires. Hansen [13] presented a number of CFD simulations for several suggested fire scenarios in underground mines. The study did not contain any validation as the scenarios were not based on any fire experiment data. Yuan et al. [14] conducted a CFD study on the carbon monoxide spread during underground mine fires. Lee and Nguyen [15] performed CFD simulations on the fire behaviour of a mining vehicle, where the input data was partially based on full-scale fire experiment results. Hansen [16] modelled the fire gas temperatures and fire gas velocities in a mine drift using a CFD model. The results from the modelling were compared with the experimental data from full-scale fire experiments.

In the following, earlier performed fire experiments are described and the resulting mass flow data are presented. The applied CFD model is briefly described together with assumptions made, mesh grid system applied etc. The mass flow rate results of the CFD model are compared with the experimental data and analysed. A discussion on the ability to predict and reproduce the throttle effect for fire scenarios underground using a CFD model is provided.

2. The throttle effect in a mine drift

An occurring fire in a mine drift will from the start generate temperatures higher than the ambient temperature, causing a buoyancy force, which is visibly detectable through the rising smoke. With an increasing fire intensity, the temperature difference between the rising smoke and the ambient air masses will increase and the buoyancy force as well. Any influencing parameters, which will cool the rising smoke – such as an increasing mine drift height or increasing ventilation flow – will thus decrease the buoyancy force. With an increasing fire intensity and an increasing temperature in the mine drift, air masses flowing past the fire site will increase in volume. This volumetric expansion will in turn cause the so-called throttle effect, where the occurrence of the throttle effect will be detected by the blockage of the ventilation flow. See Fig. 1 for a sketch of the throttle effect in a mine drift.

A fire in a mine drift will undergo several different phases with varying intensity, generated temperatures, and buoyancy forces. After the ignition, the fire will enter the incipient phase with generally low intensity and less distinct buoyancy force. Gradually, the fire will grow in intensity and eventually enter the growth phase. The growth phase is distinguished by a steadily increasing heat release rate, eventually attaining the maximum fire intensity with the highest temperatures.

Hansen [5] found that for a fire in a mine drift – where a blower fan upstream of the fire provided the ventilation flow – an increasing heat release rate will increase the buoyancy force and increase the reduction in the mass flow rate. With an increase in the longitudinal ventilation velocity, the mass flow rate will initially decrease due to an increased heat release rate. With a further increase in the ventilation velocity, the maximum heat release rate will eventually occur, and any a further velocity increase will result in a mitigating effect on the mass flow rate reduction. The mitigating effect could be seen in the delayed initiation of the mass flow rate reduction, occurring only at the very highest heat release rates. Fig. 2 displays the mass flow rate ratio from one of the model-scale experiments where the mass flow – after an initial oscillation – can be seen to decrease only for the higher dimensionless heat release rates. The mass flow rate ratio is the ratio between the mass flow rate downstream of the fire to the mass flow rate upstream of the fire, where the mass flow rate upstream of the fire was taken as the average value prior to the fire. Hansen [5] proposed an average value of the Froude number of 0.8 as a possible threshold criterion for the throttle effect. The Froude number being suitable as it contains the ratio of the buoyancy head of the fire to the kinetic head of the longitudinal ventilation flow.

The actual reduction in the mass flow rate downstream of the fire was found to result from a larger decrease in the gas density (caused by the heating from the fire) compared with the increase

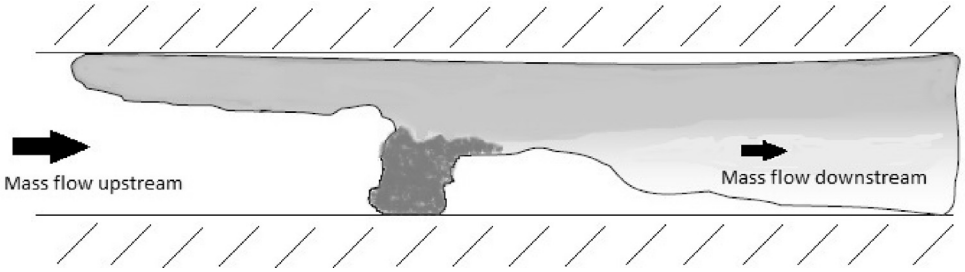

Fig. 1. The throttle effect in a mine drift.

in the flow velocity. A dimensional analysis resulted in the following equation where the mass flow rate reduction during the incipient phase and the growth phase could be reasonably well described by equation (1) [5]:

$$\frac{\dot{m}_{\text{downstream}}}{\dot{m}_{\text{upstream}}} = 1.13\left(0.807\left(\frac{\dot{Q}}{\rho_{\text{upstream}}\, c_p\, T_a\, g^{\frac{1}{2}} D_h^{\frac{5}{2}}}\right)^{-0.023}\left(\frac{u_{c,\text{upstream}}^2}{g\, D_h}\right)^{-0.007} - 0.794\right)^{0.062} \quad (1)$$

where $\dot{m}_{\text{downstream}}$ is the mass flow downstream of the fire [kg/s], $\dot{m}_{\text{upstream}}$ is the mass flow rate upstream of the fire [kg/s], $\dot{Q}$ is the heat release rate [kW], ρ_{upstream} is the gas density upstream of the fire [kg/m^3], c_p is the specific heat [kJ/kg K], T_a is the ambient air temperature [K], g is the gravitational constant (set to 9.81 m/s^2), D_h is the hydraulic diameter of the mine drift [m] and $u_{c,\text{upstream}}$ is the centreline flow velocity upstream of the fire [m/s].

Litton et al. [4] conducted fire experiments, investigating the throttle effect with different ventilation conditions compared with Hansen [5], i.e., an exhaust fan was used. A maximum 10–11% reduction in the total airflow and a 29% reduction in the intake airflow were recorded. The flow results were thus also found to differ between the two sets of experiments and the difference could be explained by the different experimental conditions. Litton et al. [4] used an exhaust fan, where the exhaust ventilation velocity was pre-set, and the intake velocity was measured. A threshold criterion – for the throttling effect – based on a modified Froude number was also proposed by Litton et al. [4].

3. Methodology

3.1. Fire experiments in a model-scale mine drift

The result from the CFD modelling was validated and compared with the corresponding result from

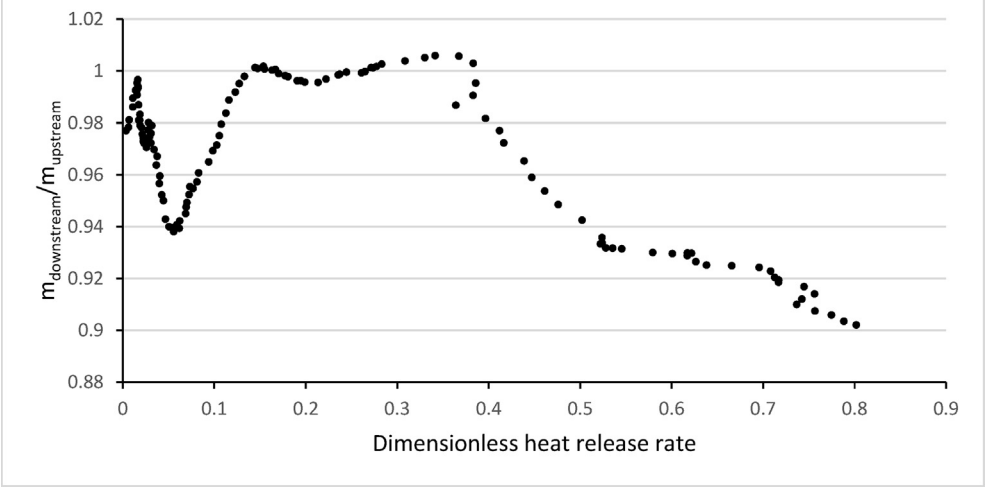

Fig. 2. The mass flow rate ratio of experiment #12 as a function of the dimensionless heat release rate [5].

fire experiments in a model-scale mine drift [17]. The dimensions of the model-scale mine drift were 10 m in length, 0.6 m in width and 0.4 m in height. The experiments consisted of a total of 12 experiments, involving single or multiple piles of scaled down wooden pallets and where each pile consisted of five wooden pallets. The heat release rate was calculated based upon a method by Newman [18] and as it is important to model the heat release rate of each pile of pallets correctly – applying the calculated heat release rate from the experiments – mainly the experiments involving only a single pile were used during the analysis. Four experiments were conducted where only a single pile of pallets was used as fire load and where only the longitudinal ventilation velocity was varied: 0.3 m/s (experiment #1 and experiment #2), 0.6 m/s (experiment #4) and 0.9 m/s (experiment #12).

Figure 3 displays the layout of the model-scale mine drift with the attached measuring devices and with two separate fuel loads. In the experiments involving a single pile of pallets, the pile of pallets was always placed at the positioned marked "W" in Fig. 3. The pile of pallets was positioned with the long side facing the longitudinal ventilation flow. Not seen in Fig. 3 is an exhaust duct – with a diameter of 0.26 m – positioned at the end of the mine drift. When investigating the throttle effect, the temperatures and flow velocities downstream of the fire are highly interesting. As there were uncertainties regarding the positioning of the measuring point in the duct and the configuration of the duct, mainly the temperatures and pressures measured at pile B were used throughout the analysis. The thermocouples of pile B were positioned at different heights to provide a picture of the vertical temperature distribution. The bi-directional probe at pile B would measure centreline pressure differences, providing input to the downstream centreline flow velocity calculations. Thus, explaining the reason why a single bi-directional probe at mid-height was used during the experiments.

The ventilation flow in the mine drift was provided by an electrical axial fan positioned at the entrance of the model scale mine drift. A constant and uniform volumetric flow rate was provided, using a frequency regulator. The centreline flow velocity upstream of the fire was calculated, using the measured pressure differences of the bi-directional probe positioned between the fan outlet and the fuel load at "W" as well as the temperatures measured at the thermocouple positioned above the bi-directional probe.

The centreline flow velocities were calculated using the pressure differences measured at the bi-directional probe in question as seen in equation (2) [17]:

$$u_c = \frac{1}{k}\sqrt{\frac{2\Delta p T}{\rho_a T_a}} \tag{2}$$

where k is a calibration coefficient (set equal to 1.08), the measured pressure difference – Δp is the measured pressure difference [Pa], T is the gas temperature [K], ρ_a is the density of the ambient air [kg/m^3] and T_a is the ambient air temperature [K].

Equation (3) was used for calculating the mass flow rate [17]:

$$\dot{m} = \zeta\, u_c A \frac{T_a \rho_a}{T} \tag{3}$$

where ζ is a mass flow correction factor (set equal to 0.817) and A is the cross-sectional area of the mine drift or duct [m^2].

The report by Hansen and Ingason [17] contains a detailed description of the experiments.

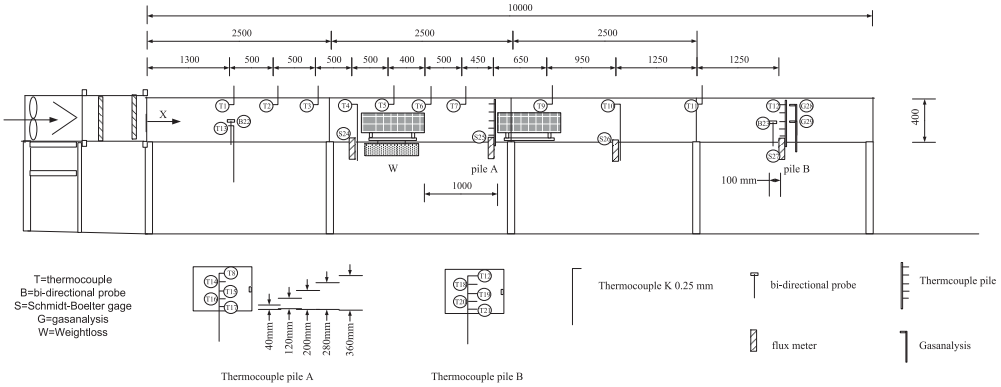

Fig. 3. Layout of the model-scale mine drift with attached thermocouples, probes, and instruments [19].

3.2. CFD modelling

Fire modelling in an underground mine could employ a mine ventilation network model, a zone model or a CFD model. A mine ventilation network model will assume an immediate and complete mixing of gases and will therefore not model a stratified flow, which was the case in the experiments. A CFD model can be used to predict ventilation flows, heat transfer, pressure etc. during a fire. Simulations with a CFD model may be very lengthy in time and require considerable computational resources. Thus, CFD modelling will generally be conducted for a limited part of the mine to decrease the computational requirements and the time required. A CFD model rests on the fundamental laws of fluid mechanics and heat transfer found in the laws of conservation mass, momentum (rate of change of momentum equals the sum of the forces on a fluid particle) and energy (rate of change of energy is equal to the sum of the rate of heat addition to and the rate of work performed on a fluid particle).

Fires are generally turbulent and to resolve the turbulent flows CFD models uses turbulence models. Large Eddy Simulation (LES) is one example, where it is assumed that most of the mixing is caused by turbulent eddies large enough to be predicted by fluid mechanics equations. The smaller eddies are assumed to be adequately approximated by appropriate models. The turbulence can also be solved using a Direct Numerical Simulation (DNS) where spatial and temporal scales are resolved for the given application. DNS requires a numerical mesh fine enough to solve the unsteady Navier–Stokes equations and is very computationally demanding compared with LES.

3.2.1. FDS and input/output parameters

When performing the fire simulations, the Fire Dynamics Simulator (FDS) was chosen as CFD model, as FDS is a commonly used CFD model when simulating fire scenarios. FDS is found suitable for the low-speed, thermally driven flow occurring during a fire. The specific version of FDS was version 6.7.5 [20].

When performing fire modelling with a CFD model, the grid size of the mesh will be of outmost importance with respect to the validation of the output results. A too large grid size will reduce the accuracy and the confidence in the output results. McGrattan et al. [20] set forward the following resolution of the fire plume flow field found in equation (4), described by the characteristic fire diameter:

$$D^* = \left(\frac{\dot{Q}}{\rho_a c_p T_a \sqrt{g}}\right)^{2/5} \tag{4}$$

Applying the characteristic fire diameter, Li et al. [21] showed that a mesh grid size smaller than the range: $0.075D^* - 0.1D^*$ will result in no differences in the output results. Experiments #1 and #2 resulted in the lowest heat release rates of the four experiments, with an average heat release rate of approximately 50 kW (where mostly the heat release rates exceeding the average value were of interest with respect to the mass flow). Applying the given characteristic fire diameter range, a mesh grid size of 0.02 m was chosen. A single mesh grid size was applied throughout the entire domain.

As the grid size was too large for the DNS mode (the DNS mode is suitable for a grid size of approximately 1 mm), the LES mode was chosen for all simulations.

The simulated time was set to 8 min as this time length would encompass the growth phase and the initiation of the decaying phase of the experiments, thus capturing the most critical stages of the fires.

The simulations were started 2 min prior to ignition, coinciding with the start of the measurements in the experiments.

The fuel in the fire experiments consisted of single piles of scaled down pine pallets (the pile consisted of five individual pallets). The dimensions of each pallet can be found in the report by Hansen and Ingason [17]. The following fuel parameters for pine were applied in FDS:

- Thermal conductivity: 0.11 W/m K [22]
- Specific heat: 1.35 kJ/kg K [22]
- Heat of combustion: 18100 kJ/kg [17]
- Density: 370 kg/m^3 [22]

All the surface areas of the pallets exposed to the surrounding air were defined as burning surfaces in the simulations.

To model the heat release rate of the four experiments, the heat release rate per unit area (HRRPUA) model was selected as pyrolysis model and where the calculated heat release rates of the experiments were used as input. The total surface area of a pile of pallets was calculated (areas exposed to surrounding air) and a ramp function was used in FDS to describe the heat release rate per unit surface area as a function of time. Figure 4 displays the heat release rates of the four model scale experiments.

As the heat release rate from the experiments actually occurred somewhat earlier than the recorded data further downstream from which the heat

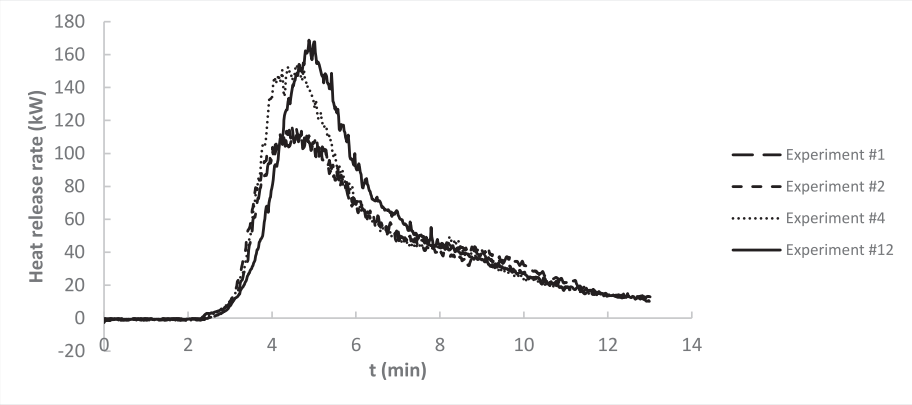

Fig. 4. The heat release rates of the model scale experiments involving a single pile of wooden pallets.

release rate was calculated from, the time difference had to be accounted for when presenting the FDS results. The time difference was calculated by dividing the distance between the fire and the measuring point by the average ventilation flow velocity.

The calculated total heat release rate of the experiments involving multiple piles of pallets can only to some extent be correctly allocated to the individual piles. In these cases, the heat release rate of the experiment involving only a single pile of pallets was subtracted from the total heat release rate until the third pile was ignited – also adding the time delay between the fire and the measuring point – to obtain the heat release rate of the second pile of pallets.

The radiative heat transfer was set in default operation, solving the radiation transport equation for a gray gas. As the flame length in a mine drift with longitudinal ventilation can be substantial, the radiative fraction was set to 0.45 in some simulations – as opposed to the default value of 0.35 – to investigate the impact on the output results. Furthermore, an earlier study has also pointed out the radiative fraction as an error source when modelling the fire gas temperatures [16].

The surrounding surfaces of the model scale mine drift consisted of 15 mm thick Promatect boards and 5 mm thick window glazes. Table 1 displays the surface parameters of the two materials. In the case of the window glaze, surface parameters for a borosilicate glass were assumed.

Table 1. The surface parameters of the Promatect boards and the window glazes.

Type of material	Promatect H	Window glaze
Conductivity [W/m K]	0.175 [17]	1.0 [23]
Specific heat [kJ/kg K]	1.13 [17]	0.80 [23]
Density [kg/m^3]	870 [17]	2350 [23]

The surface roughness will have an impact on the heat transfer from the fire gases to the surrounding boards and window surfaces as well as any other obstacle surfaces in the direction of the ventilation flow. The surface roughness of the Promatect board surfaces and the sanded wooden surfaces of the pallets was set to 0.0001 m. The window glazes were assumed to have no surface roughness.

In some of the simulations, a loglaw (logarithmic law) wall model was applied to investigate the impact of the boundary layer on the turbulent flow. The loglaw function is aimed at simulating the turbulent transport close to for example the board and window surfaces, applying less computationally demanding algebraic functions. The shear at the surfaces is assumed to be constant. When applying the loglaw function, the resulting convective heat transfer may be affected.

The fan in each experiment provided a constant and uniform volumetric flow rate. In each experiment, the fan was running 2 min prior to the ignition and the average ventilation flow velocity (at the upstream bi-directional probe) during the initial 2 min was used as the constant ventilation velocity in the FDS simulations. The average flow velocity prior to the fire was used in the modelling as the flow velocity measurements during the fire displayed erratic behaviour due to increased eddy formations at the entrance of the mine drift.

The ambient temperature of the ventilation flow was set to 22 °C in all simulations.

The inlet (at the position of the fan) was set to velocity boundary. The duct – following upon the model scale mine drift – was also included in the simulated domain. The diameter of the duct was 0.26 m and the outlet boundary condition was modelled as a HVAC duct connected to the ambient.

When calculating the resulting downstream mass flow rate, the temperature and the velocity measuring points positioned in accordance with thermocouple pile B and the bi-directional probe (see Fig. 1) were used in the FDS simulations.

The flow picture in the model-scale mine drift will be distinguished by localized eddy formations close to the entrance. Further downstream – with the establishing of the hydrodynamically fully developed region – the pressure gradient and shear stress in the flow will be in balance and the eddies will decay. When calculating the hydrodynamic entrance length of the various experiments it was found that only in experiments #1 and #2 was pile B positioned in the hydrodynamically fully developed region. Therefore, in the other experiments the model-scale mine drift was extended in length in the simulations so that the measuring point would be in the developed region. The analysis of the other experiments was mainly of qualitative nature, comparing for example trends.

Additional measuring points – recording the flow velocity – were added at pile B during simulations of experiments #1 and #2 to further analyse the flow velocity at pile B and the thermal stratification. For experiment #1, additional measuring points (temperature) were positioned at pile A in accordance with the experimental set up (see Fig. 3) to analyse the thermal stratification.

4. Results and discussion

When comparing the modelling results with the experimental results for the same experiment, the least squares method was applied to find the input configuration with the minimum residual sum of squares. When presenting the modelled under/overprediction compared with the experimental result, the under/overprediction was given in percentage.

4.1. Experiment #1

4.1.1. Base case

Figure 5 displays the measured and modelled mass flow rate downstream of the fire at pile B, where the base case input values were used in the FDS modelling. The modelled mass flow rate matched the measured, experimental mass flow rate very well up until the early stages of the throttle effect. The modelled mass flow rate matches the experimental results during the initiation of the throttle effect, but when the experimental mass flow rate starts to level out, the modelled mass flow rate continues to decrease. During the period with maximum throttle effect, the modelled decrease in the mass flow rate is almost three times as high as the measured decrease. When the measured mass flow rate starts to increase, the modelled mass flow rate follows the changes of the measured mass flow rate very well but from much lower levels. Where the measured mass flow rate displays similar values prior to the occurrence of the throttle effect, the modelled mass flow rate displays values much lower as if the throttle effect would still occur. The modelled results clearly over predict the throttle effect throughout most parts of the fire, resulting in too low mass flow rates.

Figures 6–9 display the measured and modelled temperatures at various thermocouples at pile B. The modelled temperatures at thermocouple Tc12 – with the longest distance to the floor: 0.36 m – clearly under predicts the gas temperatures as can be seen in Fig. 6. The under prediction is most evident during the period with the maximum heat release rate.

Starting from thermocouple Tc18 (see Fig. 7) – at 0.28 m above the floor – and downwards (see Fig. 8), the modelled gas temperatures are clearly over predicted when comparing with the measured

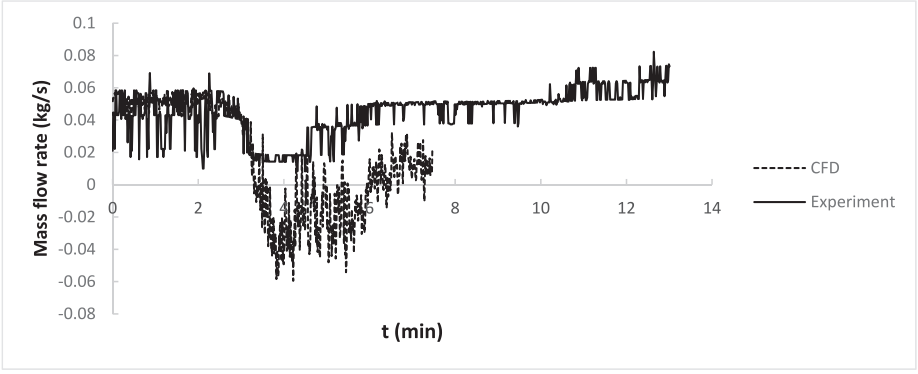

Fig. 5. The measured and modelled (applying base case input values) mass flow rate of experiment #1.

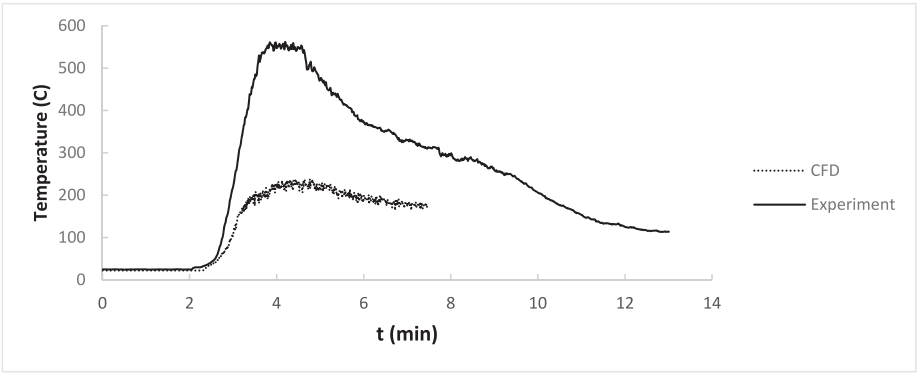

Fig. 6. The measured and modelled temperature at thermocouple Tc12 – experiment #1.

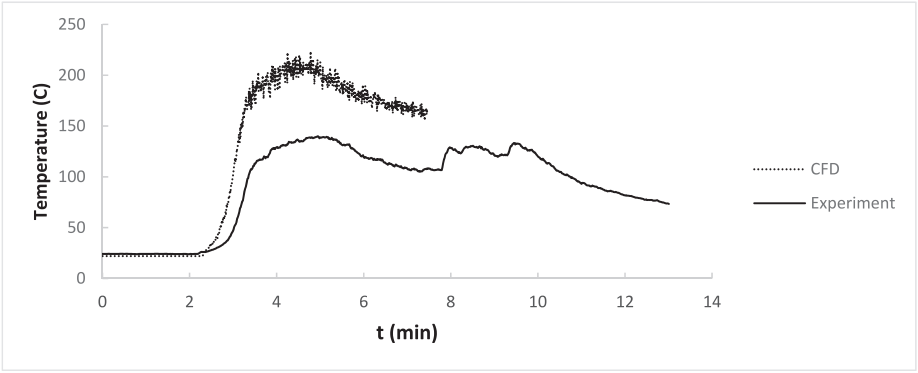

Fig. 7. The measured and modelled temperature at thermocouple Tc18 – experiment #1.

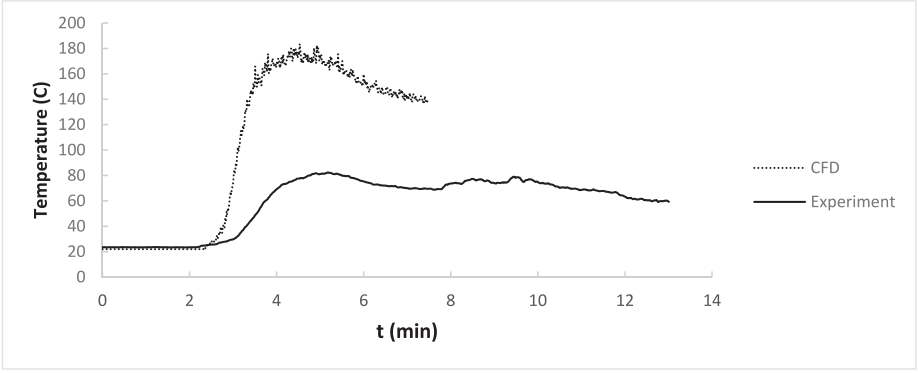

Fig. 8. The measured and modelled temperature at thermocouple Tc19 – experiment #1.

values. The degree of over prediction increases with decreasing height above the floor.

The over prediction is most evident for thermocouple Tc20 – at 0.12 m above the floor – where the modelled temperature is almost four times as high as the measured temperature (see Fig. 9).

The under prediction of the temperature at thermocouple Tc12 and the over prediction of the temperatures at thermocouples at lower levels indicates the difficulty of the FDS simulations to correctly model the occurring stratification in the model-scale mine drift. If applying the expressions by Newman [18] to classify the degree of stratification at pile B, the modelled results indicated region II (intermediate stratification) whereas the experimental results indicated region I (severe stratification).

Figure 10 displays the average gas temperature at pile B and as can be seen the modelled temperature matches the measured temperature very well up to 4 min into the experiment. After 4 min, the model

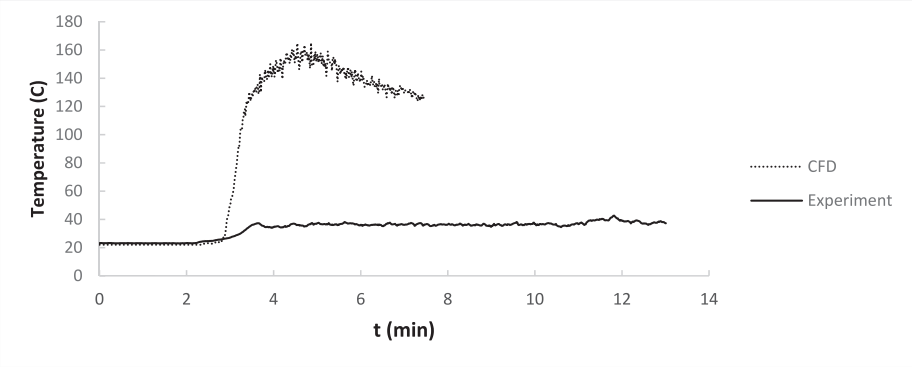

Fig. 9. The measured and modelled temperature at thermocouple Tc20 – experiment #1.

starts to over predict the temperature compared to the measured temperature. The match is due to that the over prediction of the temperatures at the lower thermocouples is cancelled by the under prediction of the temperature at thermocouple Tc12. The resulting average gas temperature thus balance the inability to predict the gas temperature at the individual thermocouples.

Earlier fire modelling studies in tunnels and mine drifts with longitudinal ventilation have also encountered the issue of over and under prediction of gas temperatures as well as difficulties when simulating thermal stratification in CFD simulations [16,21]. Li et al. [21] performed some modelling verification of model-scale tests performed in a tunnel with similar geometrical dimensions compared to the model-scale mine drift. The simulated vertical temperature distribution was found to match well with the measured results. The applied fire source during the verification was constantly at 9.45 kW, thus a fire source differing substantially compared with the pallet fires in the mine drift with transient heat release rates at generally much higher levels. Hansen [16] found that the CFD model clearly over predicted the fire gas temperatures at lower levels in a full-scale mine drift during periods with high fire growth rate and heat release rates. If applying the scaling model for the heat release rate in the model-scale experiments, equation (5) would be used:

$$\dot{Q}_F = \dot{Q}_M \left(\frac{L_F}{L_M} \right)^{5/2} \tag{5}$$

where L is the length [m], F is an index relating to full scale (which was set to 15) and M is an index relating to model scale (which was set to 1). A heat release rate of for example 20 kW in the model-scale experiments (if studying Fig. 4, it would represent the stage when the heat release rate would initiate a rapid fire growth) would be equivalent to approximately 17 MW in the full-scale experiments which is a heat release rate typically found during the phase with higher fire growth rate and heat release rate. Thus, the FDS modelling of the model-scale experiments would encounter the same difficulties when predicting the thermal stratification starting from the initiation of the throttle effect. The difficulty in predicting the thermal stratification (and the throttle effect) for periods with higher fire

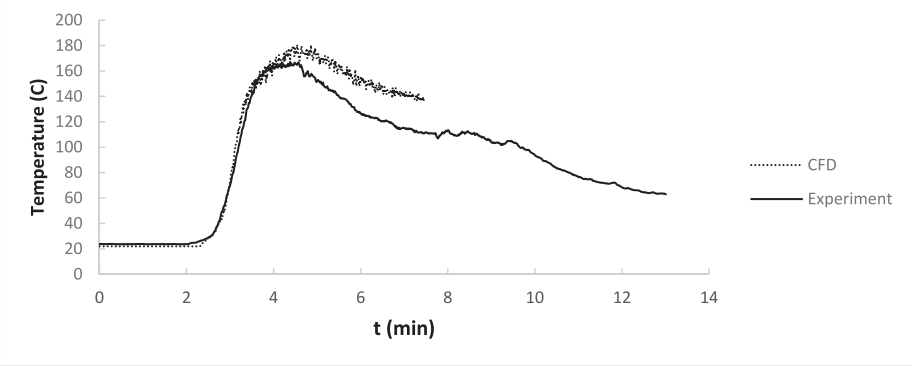

Fig. 10. The measured and modelled average temperature at pile B – experiment #1.

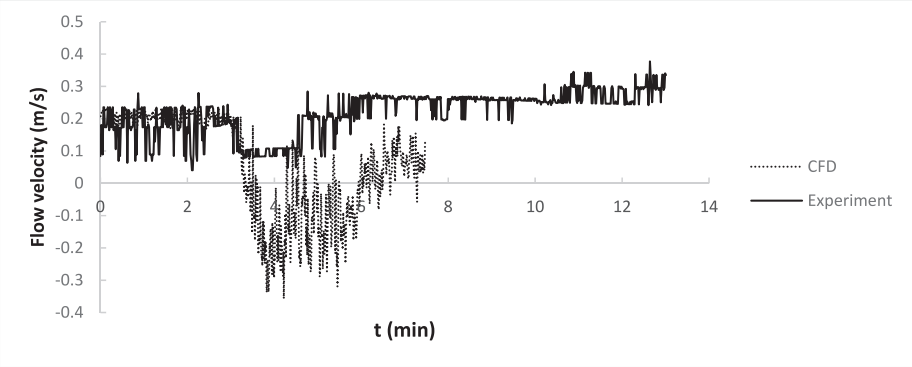

Fig. 11. The measured and modelled flow velocity at pile B – experiment #1.

growth rates and heat release rates poses a problem as higher growth rates and heat release rates would generally be required to cause the throttle effect.

The failed prediction of the thermal stratification is due to the inability to model the heat losses of the flowing fire gases correctly. This inability can be seen in the over prediction of the heat losses of the fire gases near the ceiling, resulting in a too low degree of stratification and fire gases with too high temperatures at the lower levels.

The flow velocities at the bi-directional probe at pile B can be found in Fig. 11. The appearance of the flow velocities is more or less identical with the measured and modelled mass flow rate, which is due to that the decrease in the flow velocity was significantly larger than the decrease in the gas density. Thus, the variations of the flow velocity largely dictated the variations of the mass flow rate. The over prediction of the throttle effect was therefore mostly due to the under prediction of the flow velocity. The bi-directional probe at pile B was positioned at the same height as thermocouple Tc19 and the over prediction of the gas temperature at Tc19 (see Fig. 8) due to the failed prediction of the thermal stratification would also result in a failure to predict the flow velocity at the same height for the same reason. An over prediction of the temperature would lead to an over predicted buoyancy force and throttle effect.

The use of a single measuring point to model a flow velocity, which in turn is used to calculate the mass flow rate across the entire cross-section raises some questions on the output results. An average flow velocity would account for the variations along the cross-section and the thermal stratification. Furthermore, an average flow velocity would take advantage of the earlier match between the measured and the modelled average gas temperature (see Fig. 10) and the existing relationship between the average gas temperature and average flow velocity in a duct found in equation (6):

$$\overline{u}_{\text{downstream}} = u_{c,\text{upstream}} \cdot \frac{\overline{T}_{\text{downstream}}}{T_a} \tag{6}$$

where $\overline{u}_{\text{downstream}}$ is the average gas flow velocity downstream of the fire [m/s], $u_{c,\text{upstream}}$ is the centreline flow velocity upstream of the fire [m/s] and $\overline{T}_{\text{downstream}}$ is the average gas temperature downstream of the fire [K].

Thus, applying an average flow velocity would possibly eliminate some of the uncertainties and differences. An additional simulation was performed on experiment #1, using the base case input values and adding additional velocity measurement points at equivalent positions as the thermocouples of pile B. As can be seen in Fig. 12, the result from the FDS modelling matches the measured mass flow rate very well except for the latter part of the simulation (the residual sum of squares was only 15% of the corresponding sum using a single measuring point). During the latter part, the mass flow rates of the experiment attain the same levels as prior to the fire whereas the modelled mass flow rates are found at lower levels. Some of the over prediction of the throttle effect may be attributed to the over prediction of the average gas temperature (see Fig. 10) after 4 min, but this would only partially explain the difference.

At the initiation of the throttle effect, the modelled mass flow rate in Fig. 12 can be seen to initially increase before rapidly decrease. This hump in the modelled mass flow rate cannot be found in the measured mass flow rate at pile B or in the duct (see Fig. 13). The hump in the mass flow rate is caused by the sudden increase in the flow velocities at the measuring points 0.36 and 0.28 m above the floor, clearly exceeding the corresponding decrease in the three lower measuring points. The model seemingly

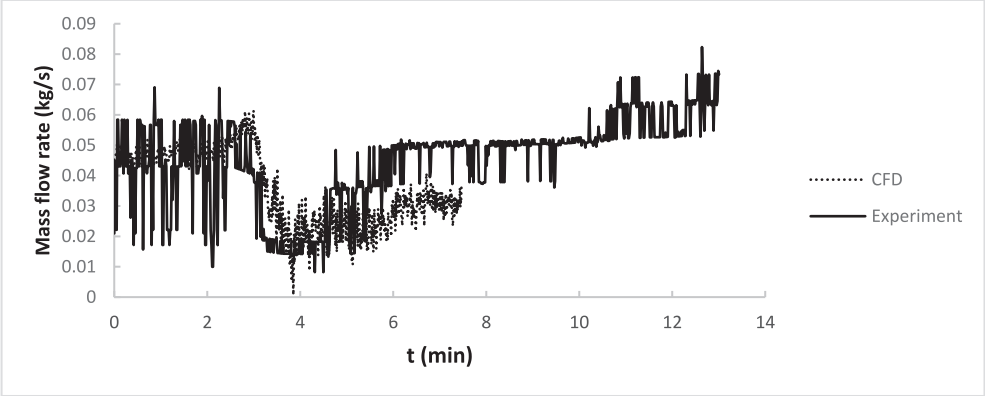

Fig. 12. The measured and modelled mass flow rate of experiment #1, applying multiple velocity measurements at pile B.

failed to predict the transient period when the throttle effect initiates – with increase in the fire growth rate and heat release rate – and changes occur in the thermal stratification.

Would the mass flow rate actually bounce back to the initial levels as quickly as seen in Fig. 12? Given the thermal stratification and that the measured mass flow rate was based on only one measuring point, the mass flow ratio in the duct (see Fig. 13) was studied for possible clues. The gas temperature and flow velocity in the duct could be expected to have a uniform appearance, as the thermal stratification would have decreased due to the mixing in the duct. The initiation of the throttle effect takes place somewhat later in the duct compared to the throttle effect recorded at pile B, which is expected due to the distance from pile B to the measuring point in the duct. As seen in Fig. 13, it is not until after almost 8 min that the mass flow rate regains the same levels as prior to the fire. The development of the mass flow rate in the duct is therefore very much in line with the modelled mass flow rate in Fig. 12.

Overall, it would seem that the use of multiple measuring points – for both the temperature and the velocity – could mitigate the uncertainties of the modelled thermal stratification and possibly increase the confidence in the modelled mass flow rates. Nevertheless, the issue of thermal stratification will have to be handled carefully during CFD simulations.

When studying the experimental values at pile B and in the duct, the underlying mechanism causing the reduced mass flow rate seemed to change. At pile B the reduced mass flow rate was found to be caused by the decrease in both the flow velocity and the gas density, whereas in the duct the reduction was solely caused by the decrease in the gas density. Given that the single bi-directional probe at pile B was positioned at mid-height, the resulting flow velocities at the probe would fail to account for the higher flow velocities closer to the ceiling. Still, further studies into the transient nature of the throttle effect will be of great interest.

4.1.2. Radiative fraction set to 0.45

The simulation with a radiative fraction of 0.45 resulted in the lowest residual sum of squares for experiment #1 – when using a single flow velocity measuring point. The resulting sum was more than

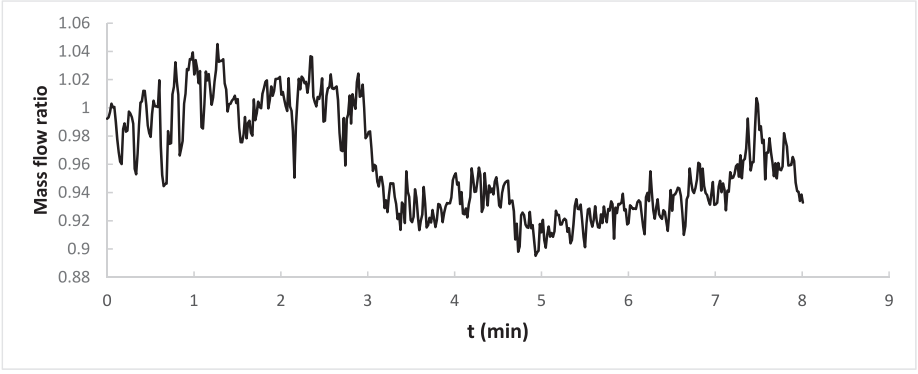

Fig. 13. The mass flow rate ratio in the duct – experiment #1.

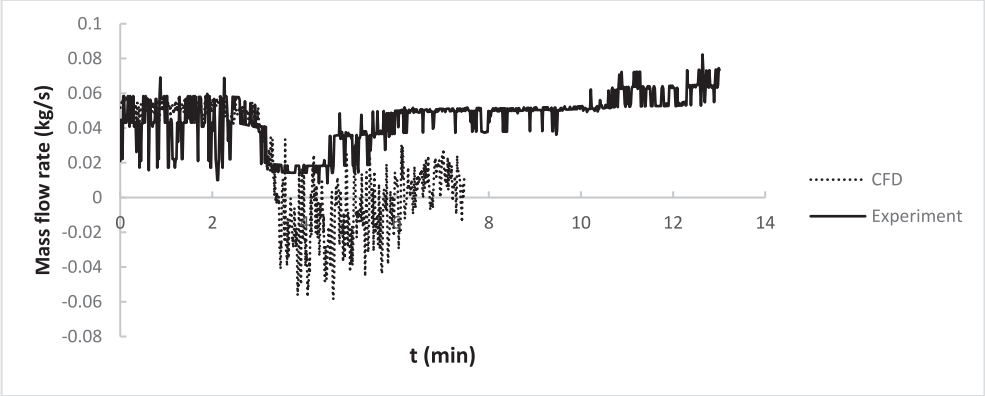

Fig. 14. The measured and modelled (applying a radiative fraction of 0.45) mass flow rate of experiment #1.

10% lower compared to the corresponding simulation using base case values. Still, during the period with maximum throttle effect, the decrease in the mass flow rate was approximately twice as high as the measured mass flow rate (see Fig. 14). The underlying reason for the improved result was foremost an increased flow velocity during the time period with a distinct throttle effect. The simulation otherwise displayed the same results as the simulation using base case input values.

An increased radiative fraction will indicate a decreased convective fraction, which in turn will lead to a decreased buoyancy force and a decreased throttle effect. This is seen in the increasing flow velocity.

Another simulation was performed on experiment #1, using a radiative fraction of 0.45 and adding additional measurement points of the velocity at corresponding positions as the thermocouples at pile B. It was found that the result was more or less identical to the corresponding simulation using base case values. Applying multiple measuring points and either the base case input values or a higher radiative fraction would therefore result in the overall closest match for experiment #1.

4.1.3. Loglaw wall function

The simulation with a loglaw wall model resulted in a slightly higher (approximately 1%) residual sum of squares compared to the simulation where base case values were applied. The worsened result can be seen in the sharper decrease in the mass flow rate and flow velocity during the initiation of the throttle effect (see Fig. 15). Applying a loglaw wall model to account for the boundary layer of the turbulent flow did not result in any improved predictions.

4.2. Experiment #2

The only difference between experiment #1 and #2 was the additional three piles of wooden pallets found downstream in experiment #2. The longitudinal flow velocities and resulting heat release rates were more or less identical in the two experiments.

4.2.1. Base case

The simulation displayed the same tendencies as the corresponding simulation of experiment #1, i.e., the under prediction of the temperature at thermocouple Tc12, the over prediction of the temperatures at thermocouples Tc18 to Tc21, an average

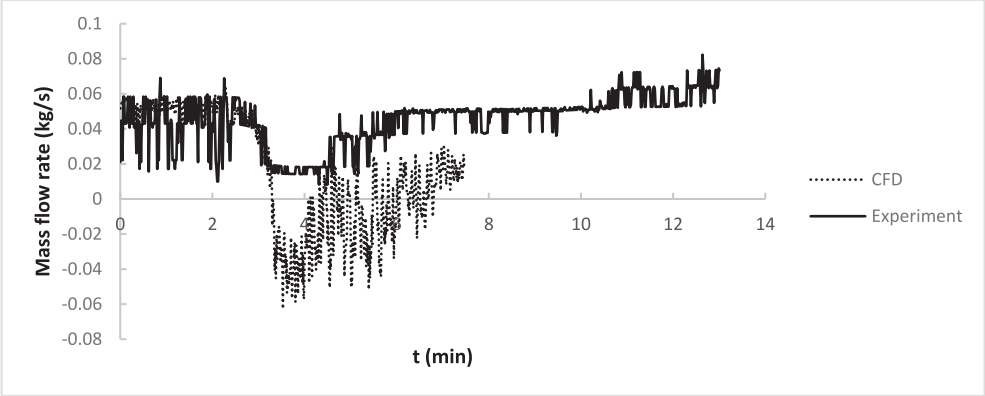

Fig. 15. The measured and modelled (applying a loglaw wall function) mass flow rate of experiment #1.

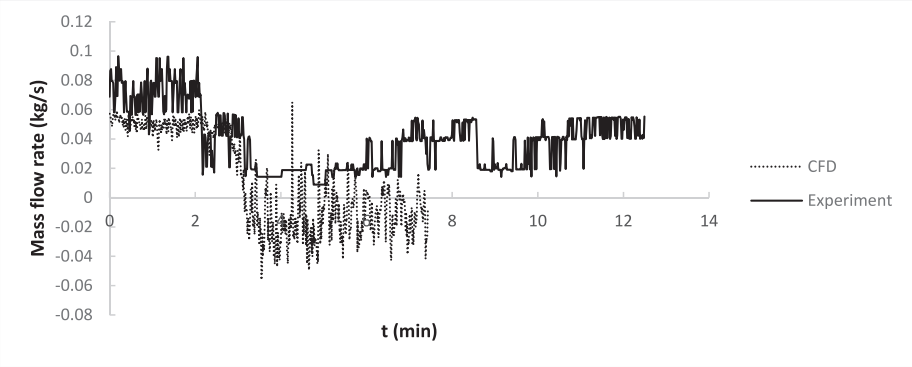

Fig. 16. The measured and modelled (applying default input parameters) mass flow rate of experiment #2.

gas temperature that initially fitted the modelled temperature very well, and the under prediction of the flow velocity at the bi-directional probe.

The simulation under predicted the mass flow rate prior to the ignition of the fire but improved the match during the early stages of the throttle effect (see Fig. 16). Same as for experiment #1, the modelled mass flow rate matched the experimental results very well during the initiation of the throttle effect, but when the experimental values start to level out, the modelled values continue to decrease. The decrease in the modelled mass flow rate during the maximum throttle effect was approximately twice as large as the measured mass flow rate decrease. When the measured mass flow rate later starts to increase, the modelled mass flow rate remains at low levels.

The failure to model the initial mass flow rate prior to the fire is most likely due to the additional piles of wooden pallets further downstream affecting the flow measurements at pile B. The corresponding mass flow rate measurements in the duct resulted in similar results for experiment #1 and #2. Thus, it would be expected that the measured mass flow rate of experiment #2 at pile B would be similar to experiment #1, which the modelled mass flow rates of experiment #2 actually predicted. This also underlines the importance when positioning the measurement points and the use of multiple measurement points, avoiding sources of error.

Same as for experiment #1, an additional simulation was performed adding additional velocity measurement points at corresponding positions as the thermocouples of pile B. The result can be seen in Fig. 17 and the modelled mass flow rate matched the measured mass flow rate throughout most of the simulation except for the pre-fire part (see reasoning above), the hump in the modelled mass flow during the initiation of the throttle effect and the latter part of the simulation. The corresponding mass flow rate in the duct did not increase after approximately 8 min but remained at lower levels, which is in line with the modelled mass flow rate found in Fig. 17. The residual sum of squares was only a third of the corresponding sum using a single measuring point.

4.2.2. Radiative fraction set to 0.45

Setting the radiative fraction to 0.45 resulted in similar results compared to the simulation using

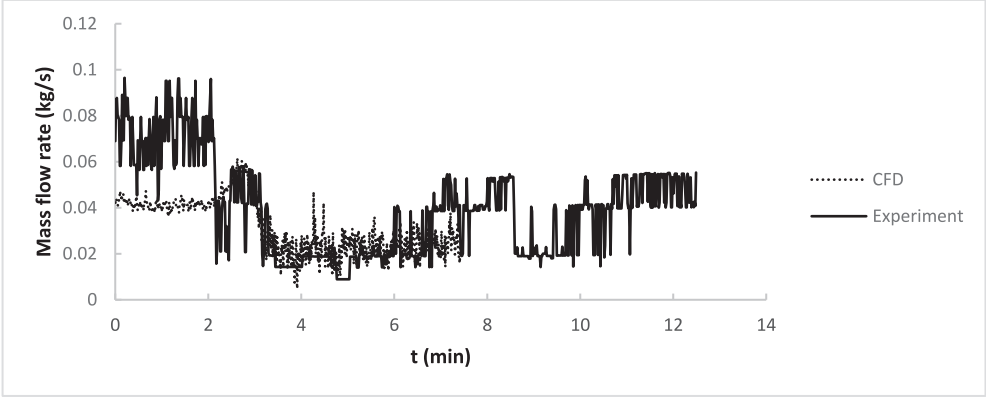

Fig. 17. The measured and modelled mass flow rate of experiment #2, applying multiple velocity measurements at pile B.

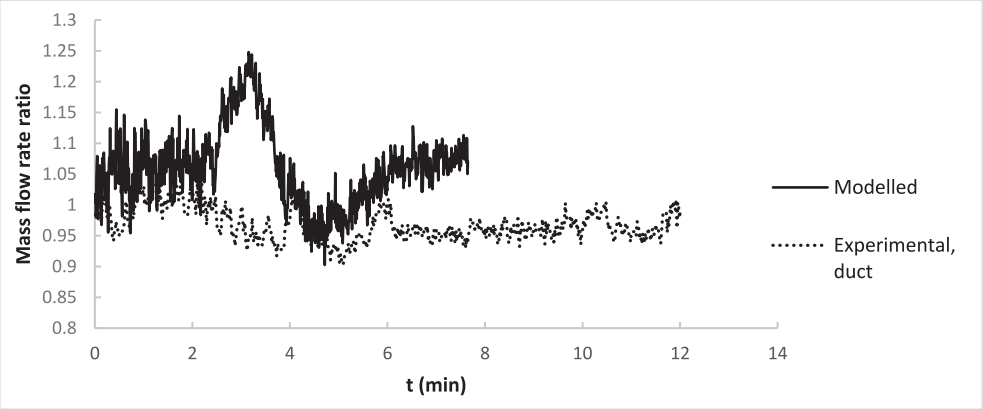

Fig. 18. The modelled mass flow rate ratio and the measured mass flow rate ratio in the duct – experiment #4.

base case values. The residual sum of squares was more or less identical for the two simulations.

The increased radiative fraction led to a somewhat decreased throttle effect during the time period following upon the maximum heat release rate (see Fig. 4). Prior to the maximum heat release rate, the throttle effect increased only marginally. Therefore, the increased radiative fraction did not result in an overall decrease in the throttle effect as in experiment #1. A virtually unchanged buoyancy force compared to the base case was the explanation.

4.2.3. Loglaw wall function

The lowest residual sum of squares for experiment #2 – using a single flow velocity measuring point – was received when applying the loglaw wall model. The resulting sum was almost 15% lower compared to the other two simulations and where the better fitted values was foremost due to increased flow velocities. The turbulence transport model was seemingly more successful in modelling the turbulence associated with additional piles of pallets and wooden surfaces. Still, the modelled decrease in the mass flow rate – during the maximum throttle effect – was approximately twice as large as the measured mass flow rate decrease.

Another simulation was performed on experiment #2, where additional flow velocity measurement points were added at pile B. It was found that the result was more or less identical to the corresponding simulation using base case values. Applying multiple measuring points and either the base case input values or the loglaw wall function would therefore result in the overall closest match for experiment #2.

4.3. Experiment #4

During the simulation, the mine drift was extended to 15 m in length to ensure that the measuring point (at 14.5 m) was within the hydrodynamically fully developed region.

Being mainly of qualitative nature – studying trends etc. – the analysis focused on the mass flow rate ratios of the modelled mass flow rate 14.5 m downstream of the mine drift entrance and the measured mass flow rate in the duct.

When comparing the modelled mass flow rate ratio with the measured mass flow rate ratio (see Fig. 18), the initiation of the throttle effect is poorly modelled in the FDS simulation. The distinct hump in the modelled mass flow rate ratio cannot be found in the measured mass flow rate ratio in the duct. As noted earlier in the paper, the CFD model seemingly failed to predict the throttle effect during the transient period encompassing the initiation of the throttle effect.

The modelled and measured magnitude and point in time of the maximum throttle effect were found to match well.

The modelled mass flow rate ratio was found to attain unity values after approximately 6 min, whereas the measured mass flow rate ratio in the duct increased to unity values at a much later stage.

Thus, the modelled mass flow rate ratio successfully predicted the magnitude and occurrence of the maximum throttle effect but failed to predict the initiation and the termination of the throttle effect. The failed modelling is foremost due to the difficulty in correctly predicting the thermal stratification.

4.4. Experiment #12

During the simulation, the mine drift was extended to 16 m in length to ensure that the measuring point (at 15.5 m) was within the hydrodynamically fully developed region.

When comparing the modelled mass flow rate ratio with the measured mass flow rate ratio in the

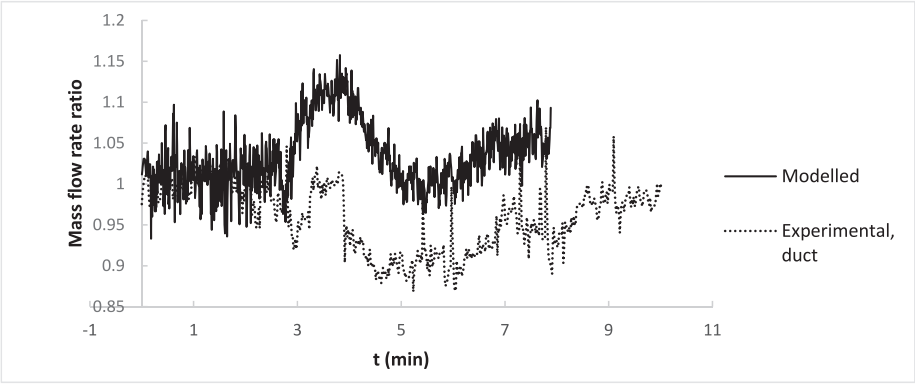

Fig. 19. The modelled mass flow rate ratio and the measured mass flow rate ratio in the duct – experiment #12.

duct (see Fig. 19), the initiation of the throttle effect is poorly matched by the modelled mass flow rate ratio. Thus, the modelled mass flow rate ratio fails to predict the delayed initiation of the throttle effect due to the increased ventilation flow velocity in experiment #12. The time period encompassing the initiation of the throttle effect is again obscured by the distinct and prolonged hump in the mass flow rate ratio.

The CFD model successfully predicts the oscillation occurring approximately 3 min into the experiment. Following upon the oscillation, the modelled mass flow rate ratio initiates the above described hump whereas the measured mass flow rate ratio briefly regains unity values before initiating the throttle effect.

The modelled and measured point in time of the maximum throttle effect was found to match well, but the magnitude of the maximum throttle effect was found to be poorly matched.

Same as for experiment #4, the termination of the throttle effect was poorly predicted by the CFD model. The difference in time was more than 1 min.

The modelled mass flow rate ratio only succeeded in predicting the time of the maximum throttle effect, but failed to predict the initiation, magnitude, and termination of the throttle effect. An additional simulation was conducted on experiment #12 where the loglaw wall model was applied to possibly improve the prediction of the turbulence connected with the increasing ventilation velocity. The magnitude of the maximum throttle effect was found to be well matched but again the initiation of the throttle effect was obscured by a hump-shaped curve in the mass flow rate ratio (though the magnitude of the hump-shaped curve decreased). The termination of the throttle effect was found to be well matched in the simulation. Clearly, the loglaw wall model improved the result of the simulation but failed to remedy the obscuration of the initiation phase.

4.5. Experiment #5

During this experiment, the longitudinal ventilation velocity was set to 0.6 m/s. The measuring point was positioned 15.5 m downstream from the mine drift entrance, extending the mine drift length to 16 m. The duration of the simulation was until the third pile of pallets was ignited, i.e. 295 s.

The modelled mass flow rate ratio matches poorly with the measured mass flow rate ratio in the duct (see Fig. 20). The initiation of the throttle effect is obscured by the hump in the simulation. Still, the simulation succeeds in predicting the magnitude of the ratio after approximately 4 min.

The modelled mass flow rate ratio displays an increase after approximately 4 min, which is not seen in the measured results in the duct. This increase is most likely due to the ignition of the second pile of pallets ($t = 231$ s [17]), affecting the modelled thermal stratification further downstream but not the measured temperature of the well mixed fire gases in the duct.

4.6. Modelling the throttle effect with a CFD model

In the simulations where multiple measuring points were applied downstream, the resulting mass flow rate contained a hump at the time when the throttle effect would commence. If studying the magnitude of the hump-shaped curves (Figs. 12 and 17–19) and comparing with the peak heat release rate of the experiments (Fig. 4), it is found that with an increase in the heat release rate the magnitude of the curve decreased. The magnitude of the curve will also decrease with increasing longitudinal flow velocity. As mentioned earlier, the hump-shaped curve is caused by the sudden increase in the flow velocity

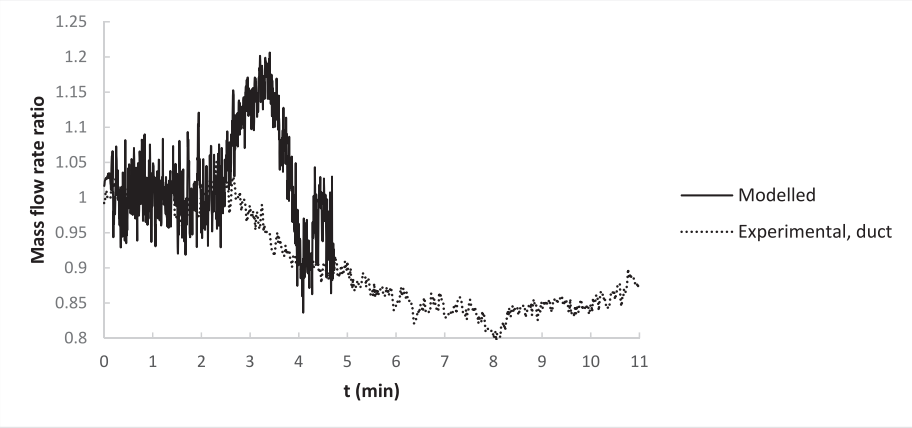

Fig. 20. The modelled mass flow rate ratio and the measured mass flow rate ratio in the duct – experiment #5.

at the higher levels of the drift and an overall increasing longitudinal flow velocity could possibly reduce the magnitude of the over prediction. Furthermore, a delayed initiation of the hump-shaped curve corresponds to a delayed initiation of the throttle effect and the fire growth phase. If studying the mass flow rate curves of experiments #1, #2, #4 and #12 and comparing with the corresponding heat release rates found in Fig. 4, it is found that the start of the hump-shaped curve coincides with the start of the rapid fire growth in the four experiments. The top of the hump-shaped curve coincides with a mid-slope position along the rapid fire growth phase and the end of the curve coincides with the point in time when the fire growth rate starts to decrease. The gradient of the heat release rate curve (i.e., the fire growth rate) and the duration of the growth phase clearly dictates the initiation and appearance of the hump-shaped curve.

To analyse the modelling of the stratification further, an additional simulation was performed on experiment #1 where the thermocouples of pile A were added as measuring points and compared with the experimental results (see Fig. 3). The results of thermocouple Tc8 positioned 0.36 m from the floor – equivalent to 0.9 times the height of the mine drift – can be found in Fig. 21.

As seen the modelled temperature resulted in a somewhat delayed temperature rise and an under predicted temperature during the peak period, but largely the model predicted the temperature development well. When comparing with the results of the corresponding thermocouple in pile B (i.e., Tc12 in Fig. 6) it is clear that in between pile A and pile B the heat losses of the fire gases are significantly over predicted. The results of thermocouple Tc14 positioned 0.28 m from the floor – equivalent to 0.7 times the height of the mine drift – can be found in Fig. 22. The over prediction of the temperature is significantly higher than the over prediction found in Fig. 7 for Tc18. Thus, the failed prediction of the thermal stratification at 0.7 times

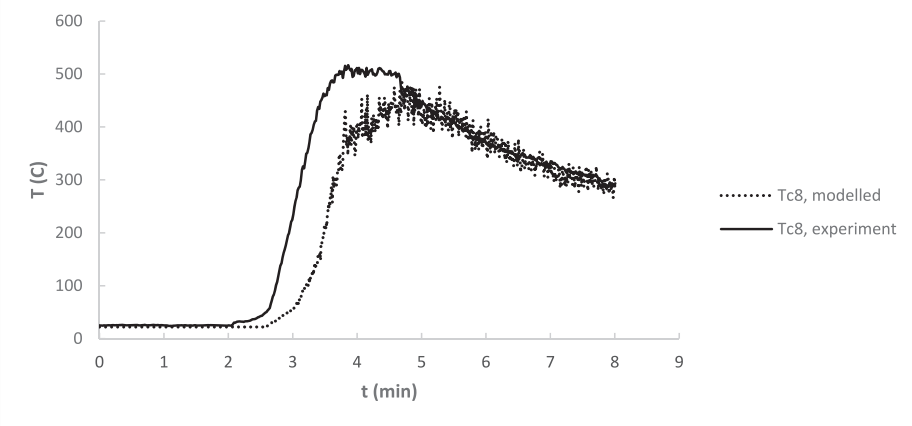

Fig. 21. The measured and modelled temperature at thermocouple Tc8 – experiment #1.

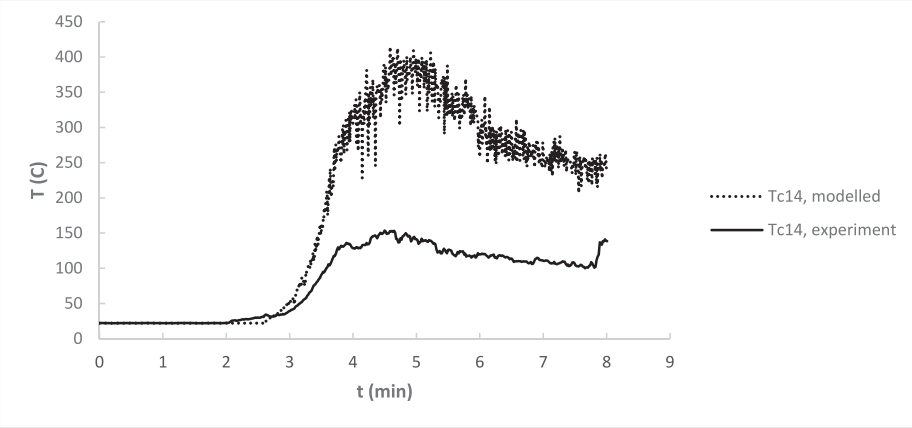

Fig. 22. The measured and modelled temperature at thermocouple Tc14 – experiment #1.

the mine drift height occurred at a short distance downstream of the fire and then persisted further downstream. The temperature distribution at 0.9 times the mine drift height fitted well at a short distance downstream of the fire, but due to over predicted heat losses further downstream the prediction of the thermal stratification again failed. The over predicted heat losses will result in increased flow velocities at the higher levels. The modelled temperatures at the lower thermocouples of pile A displayed similar results compared with pile B, i.e., clearly over predicted fire gas temperatures and thus too low degree of stratification.

Prior to full-scale fire experiments in an underground mine several CFD simulations – applying FDS – were performed to investigate the possible flow situation, smoke spread etc. during the experiments [24]. During the loader experiment a distinct throttle effect occurred, hampering the smoke extraction along the mine drift. The results from the simulations on the other hand did not give any indication of a throttle effect occurring. The fire was distinguished by a rapid fire growth and high heat release rates.

Given the importance of obtaining a fairly accurately modelled thermal stratification to in turn be able to model the throttle effect and the difficulties of the CFD model to predict the thermal stratification, it seems that at this stage the CFD model should mainly be used for qualitative analysis on the throttle effect. With further developments of the CFD model, the use could eventually extend to quantitative analysis.

The fire experiments included in this paper are all distinguished by periods of high fire growth rate and high heat release rates, which coincides with the conditions when the CFD model fails to predict the throttle effect. An earlier study managed to simulate the vertical temperature distribution with good agreement with the measured results [21]. The fire source used in the experiments was a steady-state and low heat release rate source. Quantitative analysis of the throttle effect could thus be an option for non-transient, low heat release rate fires. Given that the throttle effect will most likely occur for transient, high heat release rate fires, the use will be limited.

Among the assumptions made during the modelling work was the application of the HRRPUA-model for the pyrolysis process. The HRRPUA-model assumes a uniform heat release rate value across all fuel surfaces at all times, which will be a simplification as the different parts of the fuel item will burn with different heat release rates during the fire. Varying heat release rates – both vertically and horizontally – across the fuel item will be reflected in the temperature distribution downstream of the fire and thus also the thermal stratification. A more exact model where the changes in the heat release rates both spatially and temporally were modelled could possibly result in an improved modelling capability. This would require experimental data on the spatial variations of the heat release rates – instead of just the lumped, total heat release rate – which were not measured during the fire experiments and would be difficult to measure or estimate during an experiment. Still, more precise modelling of the heat release rate could be an area for improvement with respect to thermal stratification and the throttle effect.

5. Conclusions

A study on the possible use of a CFD model to predict the throttle effect was performed. Experimental data from fire experiments in a model-scale

mine drift and modelling results from a CFD model when analysing the possibility of reconstructing the throttle effect.

It was found that the CFD model was not able to fully reproduce the throttle effect for fire scenarios in a mine drift. The performed fire experiments were distinguished by periods of high fire growth rate and high heat release rates, where the CFD model failed to satisfactorily reproduce the occurring thermal stratification and throttle effect during the transient periods. The difficulty in predicting the throttle effect for fires with higher fire growth rates and heat release rates will be problematic as higher growth rates and heat release rates are generally required for the throttle effect to occur.

The difficulty in correctly modelling the thermal stratification was demonstrated by the under prediction of the fire gas temperature at the ceiling level and the over prediction of the temperatures at the lower levels of the mine drift. The failed prediction of the thermal stratification at the ceiling level was found to be due to the over prediction of the heat losses along the mine drift. The faulty thermal stratification at the lower heights occurred already at a short distance downstream of the fire and then persisted further downstream. Overall, the modelled results indicated intermediate stratification at the measuring point whereas the experimental results indicated severe stratification.

Given the difficulties in modelling the thermal stratification, the use of CFD models when analysing the throttle effect should be mainly of qualitative character. Quantitative analysis could possibly be performed for non-transient and low intensity fires.

As the development of CFD models is an ongoing process, future research should be focused on continuously investigating the throttle effect prediction with changes and improvements to the CFD model. Further studies should also be aimed at the transient nature of the throttle effect.

Conflicts of interest

None declared.

Ethical statement

The author state that the research was conducted according to ethical standards.

Funding body

This research received no external funding.

Acknowledgment

The author would like to thank and acknowledge the support from the Sustainable Minerals Institute, The University of Queensland.

References

[1] Hansen R, Ingason H. Heat release rates of multiple objects at varying distances. Fire Saf J 2012;52:1–10. https://doi.org/10.1016/j.firesaf.2012.03.007.
[2] Hwang CC, Chaiken RF. Effect of duct fire on the ventilation air velocity. In: Report of investigations 8311. Bureau of Mines, United States Department of Interior; 1978.
[3] Lee CK, Chaiken RF, Singer JM. Interaction between duct fires and ventilation flow: an experimental study. Combust Sci Technol 1979;20:59–72. https://doi.org/10.1080/00102207908946897.
[4] Litton CD, DeRosa M, Li J-S. Calculating fire-throttling of mine ventilation airflow. In: Report of investigations 9076. Bureau of Mines, United States Department of Interior; 1987.
[5] Hansen R. Mass flow during fire experiments in a model-scale mine drift with longitudinal ventilation. Trans Inst Min Metall Sect A 2020;129:68–81. https://doi.org/10.1080/25726668.2020.1766302.
[6] Vaitkevicius A, Carvel R, Colella F. Investigating the throttling effect in tunnel fires. Fire Technol 2016;52:1619–28. https://doi.org/10.1007/s10694-015-0512-z.
[7] Edwards JC, Hwang CC. CFD analysis of mine fire smoke spread and reverse flow conditions. NIOSH; 1999.
[8] Edwards JC, Hwang CC. CFD modelling of fire spread along combustibles in a mine entry. In: SME annual meeting and exhibit, march 27-29, St. Louis, Missouri; 2006.
[9] Edwards JC, Franks RA, Friel GF, Yuan L. Experimental and modelling investigation of the effect of ventilation on smoke rollback in a mine entry. NIOSH; 2006.
[10] Edwards JC, Friel GF, Yuan L, Franks RA. Smoke reversal interaction with diagonal airway – its elusive character. NIOSH; 2006.
[11] Friel GF, Yuan L, Edwards JC, Franks RA. Fire-generated smoke rollback through crosscut from return to intake – experimental and CFD study. NIOSH; 2006.
[12] Trevits MA, Yuan L, Teacoach KA, Valoski MP, Urosek JE. Understanding mine fire disasters by determining the characteristics of deep-seated fires. In: SME annual meeting and exhibit, february 22-25, Denver, Colorado; 2009.
[13] Hansen R. Smoke spread calculations for fires in underground mines. In: Report 2010:07. Mälardalen University; 2010.
[14] Yuan L, Zhou L, Smith AC. Modeling carbon monoxide spread in underground mine fires. Appl Therm Eng 2016;100:1319–26. https://doi.org/10.1016/j.applthermaleng.2016.03.007.
[15] Lee C, Nguyen V. A study on the fire propagation characteristics in large-opening multi-level limestone mines in Korea. Geosyst Eng 2016;19:317–36. https://doi.org/10.1080/12269328.2016.1249804.
[16] Hansen R. Modelling temperature distributions and flow conditions of fires in an underground mine drift. Geosyst Eng 2020;23:299–314. https://doi.org/10.1080/12269328.2018.1429954.
[17] Hansen R, Ingason H. Model scale fire experiments in a model tunnel with wooden pallets at varying distances. Res Rep SiST 2010;8. Västerås: Mälardalen University; 2010.
[18] Newman JS. Experimental evaluation of fire-induced stratification. Combust Flame 1984;57:33–9. https://doi.org/10.1016/0010-2180(84)90135-4.

[19] Ingason H. Model scale tunnel fire tests. SP report 2005:49. Borås. Swedish National Testing and Research Institute; 2005.
[20] McGrattan K, Hostikka S, Floyd J, McDermott R, Vanella M. Fire Dynamics simulator, user's guide (NIST special publication 1019. Gaithersburg: NIST; 2020. Sixth Edition.
[21] Li YZ, Ingason H, Lönnermark A. Numerical simulation of Runehamar tunnel fire tests. In: 6th international conference on tunnel safety and ventilation. Austria: Graz; 2012. p. 203–10.
[22] Hankalin V, Ahonen T, Raiko R. On thermal properties of a pyrolysing wood particle. Finnish-Swedish Flame Days. 2009.
[23] Bedon C. Structural glass systems under fire: overview of design issues, experimental research, and developments. Advances in Civil Engineering; 2017.
[24] Hansen R, Ingason H. Full-scale fire experiments with mining vehicles in an underground mine. In: Research report SiST 2013:2. Västerås: Mälardalen University; 2013.